AMD-Vol. 105
AD-Vol. 17

# Recent Advances in Impact Dynamics of Engineering Structures — 1989



*presented at*

THE WINTER ANNUAL MEETING OF
THE AMERICAN SOCIETY OF MECHANICAL ENGINEERS
SAN FRANCISCO, CALIFORNIA
DECEMBER 10–15, 1989

*co-sponsored by*

THE APPLIED MECHANICS DIVISION AND
THE AEROSPACE DIVISION, ASME

*edited by*

D. HUI
UNIVERSITY OF NEW ORLEANS

N. JONES
UNIVERSITY OF LIVERPOOL
UNITED KINGDOM





THE AMERICAN SOCIETY OF MECHANICAL ENGINEERS
United Engineering Center 345 East 47th Street New York, N Y 10017

# CONTENTS

# A ONE-DIMENSIONAL, TWO-PHASE FLOW MODEL FOR TAYLOR IMPACT SPECIMENS

**S. E. Jones**
U.S. Air Force Academy
Colorado Springs, Colorado

**P. P. Gillis**
University of Kentucky
Lexington, Kentucky

**J. C. Foster, Jr. and L. L. Wilson**
Eglin Air Force Base, Florida

ABSTRACT

In this paper, a simple theoretical analysis of an old problem is presented. The analysis is more complete than earlier versions, but retains the mathematical simplicity of the earlier versions. The major thrust is to separate the material response into two phases. The first phase is dominated by strain rate effects and has a variable plastic wave speed. The second phase is dominated by strain hardening effects and has a constant plastic wave speed. Estimates for dynamic yield stress, strain, strain-rate, and plastic wave speed during both phases are given. Comparisons with several experiments on OFHC copper are included.

NOTATION

$A_0$ cross-sectional area of the undeformed specimen

$A$ cross-sectional area of the deformed specimen

$D_0$ diameter of the undeformed specimen

$D$ diameter of the mushroom at the conclusion of phase I deformation

$\bar{D}$ diameter of the interface between Phases I and II

$\bar{D}_f$ diameter of the interface between Phases I and II after conclusion of the event

$D_f$ diameter of the mushroom at the conclusion of event

$e$ engineering strain

$\bar{e}$ engineering strain at the end of Phase I

$h$ distance from the undeformed anvil face to the plastic wave front

$\bar{h}$ distance from the undeformed anvil face to the plastic wave front at the end of Phase I

$\bar{h}_f$ distance from the undeformed anvil face to the phase I portion of the plastic wave front at the conclusion of the event

$\ell$ undeformed section length

$\bar{\ell}$ undeformed section length at the end of Phase I

$\ell_f$ final undeformed specimen length

$L$ original specimen length

$L_f$ final specimen length

$s$ displacement of the rear end of the specimen

$\bar{s}$ displacement of the rear end of the specimen at the end of Phase I

$s_f$ final displacement of the rear end of the specimen

$t$ time

$\bar{t}$ time at the end of Phase I

$t_f$ terminal time

$u$ speed of the plastic material at the plastic wave front

$v$ undeformed section speed

$V_0$ impact speed

$V$ volume of the material in the Phase I deformation zone

$Y_2$ average flow strength during secondary deformation

$\lambda$ secondary plastic wave speed

$\sigma$ engineering stress

$\rho$ mass density of specimen

$\dot{}$ differentiation with respect to time

## INTRODUCTION

In the 1940's engineers and scientists began to probe the dynamic mechanical properties of materials using the high speed impact of a cylindrical specimen against a massive anvil. This test is now usually called the Taylor impact test or the Taylor anvil test after Sir Geoffrey Taylor who published the first analysis of it [1]. Taylor approximated the complex real situation as a one-dimensional problem in which any effects of radial motion were assumed to be negligible. He also approximated the complex constitutive behavior of the specimen as simply a rigid, perfectly plastic material.

During the intervening years very many investigators have attempted to improve upon the original Taylor analysis. Either the mechanical equations used were made more accurate or the constitutive description of the material was made more complex. And sometimes both approaches were used simultaneously. To date, however, there has been no improvement to the Taylor theory that has achieved wide-spread acceptance. In most laboratories where the Taylor test is performed, it is interpreted using Taylor's original theory.

Beginning about 1960 there have been various computer codes written that can provide a more-or-less complete analysis of a Taylor impact test, providing the material constitutive relation is known. Nevertheless, simplified approximate analyses of the type originally offered by Taylor still have practical utility. They provide the means for a relatively fast and economical interpretation of test results. Also, they can provide a certain degree of insight into the effects various test parameters produce on the final results. For those reasons, yet another one-dimensional analysis of the Taylor impact test is presented here.

This current analysis is based upon observations emphasized by Bell [2] in 1960. Bell's experimental work on rod impact led him to the conclusion that there was a brief, initial phase of the plastic deformation entirely different from the subsequent specimen response. Here Bell's conclusion is taken as justification for a one-dimensional, but two-phase, analysis of the Taylor test. This present analysis follows the same general lines as an earlier one phase theory [3].

The differences introduced here can be summarized fairly easily. During Phase I, the rigid, plastic yield strength is allowed to be different from Phase II, the plastic wave speed (assumed constant in Phase I) is a time-dependent function, and the material particle velocity u is time-dependent. Taylor [1] approximated this particle velocity as zero throughout the entire deformation process. In this analysis the particle velocity is taken to be nonzero throughout the event.

The Phase II analysis is similar to that given earlier [3]. However, during Phase II deformation, the particle velocity u is taken to be proportional to the current undeformed section speed v.

It is believed that the two phase model provides for a more accurate basis for the analysis of the Taylor Test. Yet, the present system of equations is not a lot more complicated than that given earlier [3] or Taylor's original theory [1].

## THEORY

Consider a uniform cylindrical rod of mass density $\rho$ which impacts a rigid anvil normally and with initial speed $v_0$. The plastic deformation of the rod proceeds in two phases: the primary, or Phase I deformation phase, which is dominated by strain rate effects and high plastic wave speed and the secondary, or Phase II deformation phase, which is probably dominated by work hardening effects.

The classic Taylor [1] equation of motion of the undeformed section of the specimen has been modified by the authors to account for mass transfer across the plastic wave front. The modified equation is given by

$$\ell \dot{v} + \dot{\ell}(v-u) = \frac{\sigma}{\rho(1+e)} \qquad (1)$$

where v is the current speed of the undeformed section, $\ell$ is the current undeformed section length, $\sigma$ is the engineering stress at the plastic wave front, e is the engineering strain at the plastic wave front, and u is the particle velocity of the plastic material immediately inside the plastic wave front. Notice that under the assumption of constant volume deformation the engineering true strain e is given by $e = A_0/A - 1$. Superimposed dots denote differentiation with respect to time, t. Equation (1) is valid during both phases of the deformation process.

The characterization of each distinct phase is determined by assumptions regarding the plastic wave front motion and the particle velocity, u, inside the wave front. During Phase I, the particle velocity of the plastic material is determined by the anvil compliance, the specimen material, the impact velocity, and the current speed of the undeformed section. At the same time, the plastic wave speed is basically a function of these same quantities during this phase. Evidently, both the particle velocity behind the plastic wave front and the plastic wave speed are complicated functions of the determining variables. However, within the context of this the Eulerian plastic wave speed will be approximated in an elementary way and the anvil compliance will be neglected entirely. The particle velocity behind the plastic wave front will be developed from some simple mechanical considerations.

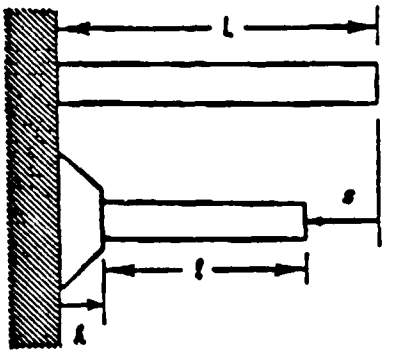


Figure 1. Schematic view showing a Taylor impact specimen of original length L which undergoes plastic deformation.

In Figure 1, the reader will note that h denotes the current observable position of the plastic wave front relative to the anvil surface. From typical film data collected on OFHC copper rods impacted against a steel anvil in the Materials Testing Laboratory at Eglin Air Force Base, Florida [4], it was noted that the plastic wave motion relative to the original anvil surface is linear after the first few microseconds of the event, as shown in Figure 2 excerpted from [4].

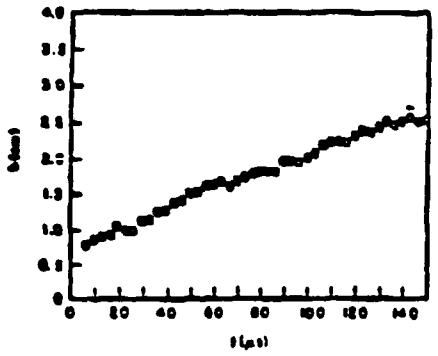

Figure 2. Graph taken from Molitoris [4] showing measurements of actual film data compiled during the impact of an OFHC copper specimen impacting a steel anvil. This data indicates that after the first few microseconds the Eulerian plastic wave speed is constant.

However, in the first few microseconds, the plastic wave is much higher than the later "steady state" value and the motion is quite nonlinear. Motivated by these observations, we are lead to consider

$$h(t) = \begin{cases} h_0 t^n, & 0 \le t \le \bar{t} \\ \lambda(t-\bar{t}) + \bar{h}, & \bar{t} \le t \le t_f \end{cases} \qquad (2)$$

where $\bar{h}$ and $\bar{t}$ are the distance of the plastic wave front and the time at the end of Phase I. $h_0$ and n are positive constants with $0 < h < 1$, and for that reason h is a continuous function of time. Applying (2) at time $\bar{t}$ gives

$$\bar{h} = h_0 \bar{t}^n \qquad (3)$$

When the event reaches conclusion, $h = h_f$ and $t = t_f$, which means that

$$\lambda = \frac{h_f - \bar{h}}{t_f - \bar{t}} \qquad (4)$$

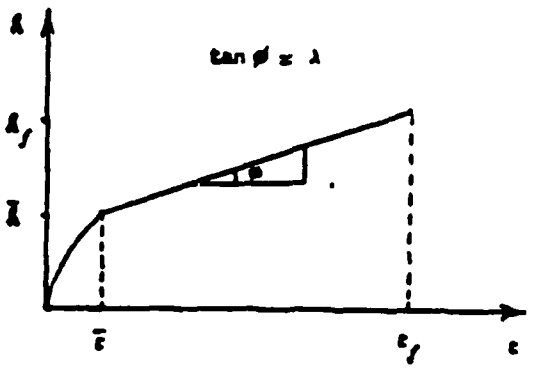


Figure 3. Graph showing the position of the plastic wave front relative to the undeformed anvil face. $\bar{h}$ and $h_f$ are distances of the plastic wave front from the anvil face at the end of Phase I and at the end of the event, respectively. $\bar{t}$ and $t_f$ are the interface and terminal times, respectively.

The kinematical analysis in this problem consists of adding the current lengths in Figure 1 to obtain

$$\ell + s + h = L \qquad (5)$$

which is valid during both phases of the deformation. Differentiation of (5) gives

$$\dot{\ell} + \dot{s} + \dot{h} = \dot{\ell} + v + \dot{h} = 0 \qquad (6)$$

which also is valid during both phases of the deformation. During Phase II, $\dot{h} = \lambda$, which reflects the constant wave front speed observed in Figure 2.

A conservation of mass relation for the plastic material can be developed by equating the distances in Figure 3. This leads to

$$e\dot{\ell} = v - u \qquad (7)$$

This is a fundamental equation in our further analysis.

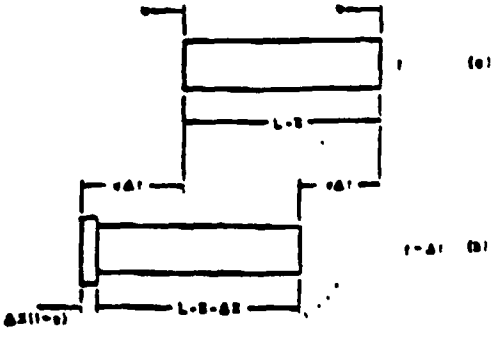

Figure 4. Schematic illustration of the rear portion of the projectile, during the time interval $\Delta t$, the front of the indicated section is displaced a distance $u\Delta t$, while the rear is displaced $v\Delta t$.

## PHASE I DEFORMATION

The initial deformation phase is characterized by rapid mushroom growth. During this deformation, it has been observed from film data on OFHC copper specimens that there is virtually no change in the velocity of the undeformed section [5]. Thus, we are motivated to assume that $v = v_0$ and $\dot{v} = 0$ throughout Phase I. This reduces equation (1) to

$$\dot{\ell}\,(v_0 - u) = \frac{\sigma}{\rho(1+e)} \tag{8}$$

during the primary deformation stage. Also, equation (6) reduces to

$$\dot{\ell} = -(v_0 + \dot{h}) \tag{9}$$

Combining this equation with (7) gives

$$e = -\frac{v_0 - u}{v_0 + \dot{h}} \tag{10}$$

for the time dependent strain directly behind the plastic wave front. Eliminating $\dot{\ell}$ and e in (8) with (9) and (10) leads to an expression for the time dependent stress during the Phase I deformation.

$$\sigma = -\rho\,(u + \dot{h})\,(v_0 - u) \tag{11}$$

where $\dot{h}$ must be specified from (2) for $t \le \bar{t}$ and u will be determined subsequently. Notice that because $0 < n < 1$, $\dot{h}$ is singular at $t = 0$. This means that the calculated stress is infinite at $t = 0$. Evidently, the stress is not infinite at impact. This conclusion is the result of the infinite propogation rate for the plastic wave front predicted by (2) at impact. The propogation rate is initially very high, but not infinite.

The particle velocity u is generally a complicated function of t. For this analysis, we will assume that it can be estimated in a very simple way. Suppose that the mushrooming region can be approximately represented by a cylindrical section (see Figure 4) with volume

$$V = Ah \tag{12}$$

where

$$A = A_0 / (1 + e) \tag{13}$$

In these equations, h is the current position of the plastic wave front, A is the current mean cross-sectional area of the mushroom, and $A_0$ is the original cross-sectional area of the specimen.

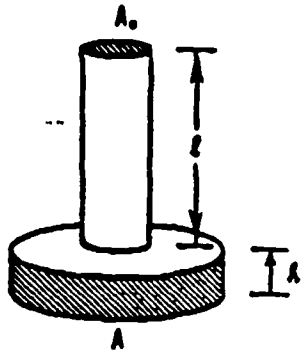


Figure 5. Idealized Phase I deformation of a rod impact specimen. The mushroom region is approximated by a cylindrical section of attitude h.

Notice that e can be eliminated from (13) by means of (10), allowing A to be expressed as

$$A = A_0 \frac{v_0 + \dot{h}}{u + \dot{h}} \tag{14}$$

and V to be expressed as

$$V = A_0\, h \frac{v_0 + \dot{h}}{u + \dot{h}} \tag{15}$$

However, the volume of the material in the plastic deformation zone must equal the volume of the material lost by the undeformed section. This means that

$$V = A_0\,(L-\ell) = A_0\,(s+h) = A_0\,(v_0 t + h) \tag{16}$$

where $s = v_0 t$ during Phase I deformation and equation (5) has been used to eliminate $\ell$. By equating (15) and (16), we obtain

$$h \frac{v_0 + \dot{h}}{u + \dot{h}} = v_0 t + h \tag{17}$$

This equation can be used to find u.

$$u = v_0 \frac{h - t\,\dot{h}}{v_0 t + h} \tag{18}$$

This relation gives the particle velocity of the material directly behind the plastic wave front as a function of time. Since we have assumed that the particle velocity of the plastic material is uniform, this relation and (10) gives us the cross-sectional area of the mushroom as a function of time.

Observing that $h = h_0 t^n$ during Phase I, reduces (18) to

$$u = v_0\, h_0\, (1-n)(v_0 t^{1-n} + h_0)^{-1} \tag{19}$$

Notice that the initial particle velocity is given by $u(0) = v_0(1-n)$ and u decreases as Phase I deformation proceeds, as shown in Figure 6.

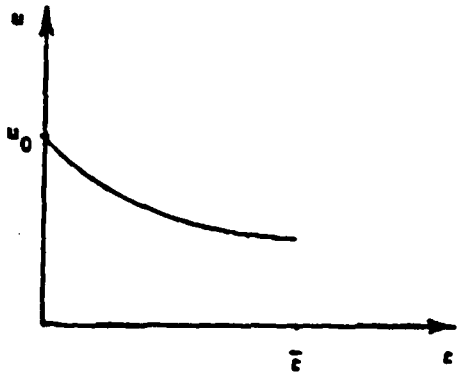


Figure 6. A typical particle velocity curve, as predicted by the theory. The particle velocity at impact is given by $u_0 = v_0$ (1-n) and decreases with time during Phase I deformation.

Equation (19) allows us to evaluate the time-dependent strain e in the cylindrical mushrooming region.

$$e = -v_0 (v_0 t^{1-n} + nh_0)(v_0 t^{1-n} + h_0)^{-1}(v_0 + nh_0 t^{n-1})^{-1} \tag{20}$$

Notice that the strain on impact is equal to zero and increases (compressively) as Phase I continues. The mushroom growth can be estimated from (20), but cannot be compared directly to the radial growth curve at the anvil interface. However, a favorable comparison can be achieved by taking the current volume of the mushroom region from (15) and replacing this cylindrical section with a conical frustrum (see Figure 7). This produces a somewhat better approximation to the radial growth curve at the anvil interface, but still underestimates the experimental observations. Nevertheless, this elementary theory for Phase I deformation qualitatively agrees fairly well with the experiment.

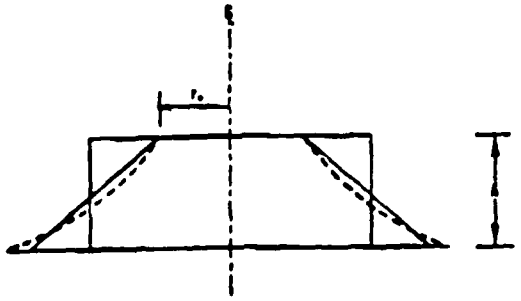


Figure 7. A schematic view of the cylindrical mushroom section with a conical frustrum approximation to the volume contained in the cylinder. At the anvil-specimen interface the actual mushroom (dashed curve) should have larger radius than the base of the conical frustrum and a much larger radius than the cylindrical section. Each has the same height and volume.

## PHASE II DEFORMATION

As indicated earlier, secondary plastic deformation is assumed to begin when the Eulerian plastic wave speed $\dot{h}$ reaches some value, say $\lambda$. During Phase II it is assumed to remain constant at this value. There will be a nonzero particle velocity u during this deformation. This particle velocity may be roughly assumed to follow the profile of the undeformed section speed during Phase II deformation. When the u curve has this type of profile, the secondary geometry for recovered specimens has the correct curvature (see Figure 8). Motivated by this, we are led to postulate a constant k such that

$$u = k\,v \tag{21}$$

for $\bar{t} \le t \le t_f$. This constant will be determined in the course of the subsequent analysis.

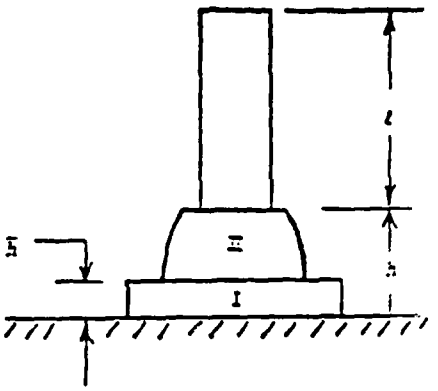


Figure 8. Idealized deformation geometry after Phase II begins. Notice the curvature of the Phase II deformation zone.

When the deformation reaches Phase II, equation (6) becomes

$$\dot{\ell} = -(\lambda + v) \tag{22}$$

Combining this with equations (7) and (21) leads to an expression for the strain

$$e = -(1-k)\frac{v}{v+\lambda} \tag{23}$$

Suppose that the average dynamic compressive yield stress during secondary deformation is $\sigma = -Y_2$. Then, equation (1) becomes

$$\ell\,\dot{v} + (1-k)\,\dot{\ell}\,v = -\frac{Y_2}{\rho}\,\frac{\lambda + v}{\lambda + kv} \tag{24}$$

Using the chain rule of differentiation, and (22) to replace $\dot{\ell}$, equation (24) transforms to

$$\ell\,\frac{dv}{d\ell} = \frac{Y_2/\rho}{\lambda + kv} - (1-k)\,v = f(v) \tag{25}$$

As the right hand side is a function of v only, this equation has separable variables. The separation and subsequent integration lead to

$$\ell = \ell_f \left[ \frac{Y_{2/\rho}}{Y_2/\rho - \lambda(1-k)v - k(1-k)v^2} \right]^{\frac{1}{2(1-k)}}$$

$$\times \left[ \frac{q-\lambda(1k)}{q+\lambda(1-k)} \; \frac{q+\lambda(1-k) + 2k(1-k)\, v}{q-\lambda(1-k) - 2k(1-k)\, v} \right]^{\frac{1}{q}} \qquad (26)$$

where $q^2 = \lambda^2 (1-k)^2 + 4 Y_2 k (1-k)/\rho$, $Y_2/\rho - \lambda(1-k) v_0 - k(1-k) v_0^2 > 0$, and $\ell_f$ is the final undeformed section length. This equation expresses $\ell$ as a function of v. When (26) and (22) are used in (24), we again find a separable differential equation. This equation has separable variables in velocity and time.

$$\ell \dot{v} = -(\lambda + v) f(v) \qquad (27)$$

where $f(v)$ is given by equation (25). Integration of (27) gives

$$t_f - t = \int_0^v \frac{\ell \, dv}{(\lambda+v) f(v)} = \frac{h_f - h}{\lambda} \qquad (28)$$

This equation gives the time as a function of the current velocity of the undeformed section during Phase II deformation.

Another integral of (27) is available through the change of variables $\dot{v} = v\, dv/ds$, but this integral is algebraically dependent on (26) and (28). We will not pursue the integration of (27) any further.

The last equation for the analysis of Phase II deformation is based on a kinematic analysis of Figure 8, using the assumption that the particle velocity of the plastic material is approximately uniform during Phase II deformation. Notice that the plastic wave front has reached a position $\bar{h}$ from the anvil surface at the end of Phase I and then travels to $\bar{h}_f$ at the conclusion of the event. This distance can be approximated by

$$\bar{h} - \bar{h}_f = \int_{\bar{t}}^{t_f} u \, dt \qquad (29)$$

By using (21), the equation can be reduced to

$$\bar{h} - \bar{h}_f = k (A_f - \bar{s}) = k(s_f - v_0 \bar{t}) \qquad (30)$$

The constant of proportionality k can be determined from this equation.

## POST-TEST MEASUREMENTS AND ESTIMATES

Figure 9 shows a profile view of a typical OFHC copper specimen which has been impacted against a 4340 steel anvil with an initial speed of 187 m/s. Beside the deformed specimen is an undeformed specimen of the same initial dimensions. Notice the distinct curvature change which occurs at the interface between Phases I and II (see Figure 10).

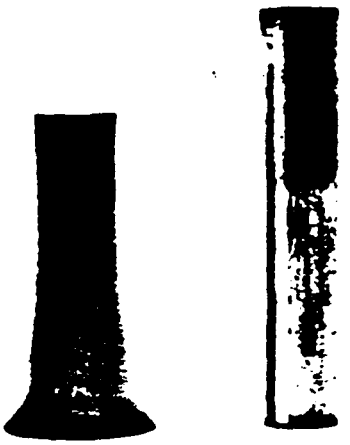

Figure 9. Profile view of actual undeformed and deformed specimens. Note the dramatic curvature change that occurs between the primary and secondary plastic deformation zones. For the deformed specimen $v_0$ = 187 m/s, L = 38 mm, and D = 7.5 mm.

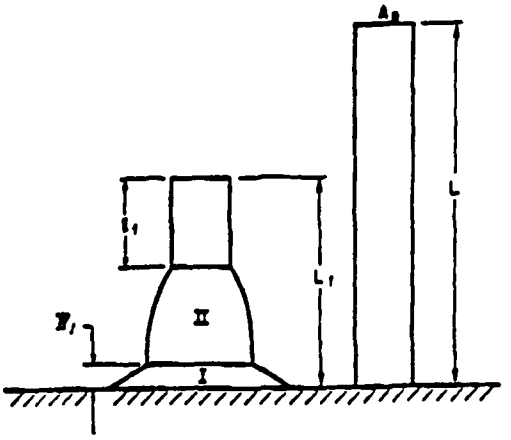


Figure 10: Schematic view of undeformed and deformed specimens, showing post-test measurements. Phases I and II have been labeled. For the actual deformed specimen shown in Figure 9, $L_f$ = 28.68 mm, $\ell_f$ = 11.68 mm, and $\bar{h}_f$ = 2.67 mm.

Figure 10 is a schematic view showing the post-test measurements. Prior to testing, the undeformed length L and cross-sectional area $A_0$ have been measured. After impact, the overall specimen length $L_f$, the length of the primary deformation region $\bar{h}_f$, and the remaining undeformed length $\ell_f$ are measured. Additionally, $\bar{D}_f$ and $D_f$, the diameter of the specimen interface and the mushroom diameter, are measured.

We will now obtain an estimate for $\bar{\ell}$ based on an elementary estimate for the volume of the mushroom. Observe, from Figure 9, that the mushroom can be well approximated by the frustrum of a cone. Estimates of this type do not originate with us (see [8] or [9]), but, within the context of this paper, they are new. In terms of the diameter of the mushroom $D_f$ and the interface diameter $\bar{D}_f$, the volume of the material in the Phase I deformation zone at the end of the event is

$$V = \frac{1}{12} \pi \bar{h}_f D_f^2 \frac{1 - \bar{D}_f^3/D_f^3}{1 - \bar{D}_f/D_f} \tag{31}$$

An interesting observation can now be made regarding the Phase I deformation zone. The mushroom region undergoes considerable deformation after the completion of Phase I (see Figure 11). However, in spite of this, the volume contained in the mushroom of the recovered specimen is approximately the same as the volume of the Phase I deformation zone at the completion of Phase I. Confirmation of this fact has been found through a comparison of the volume estimated by (31) and the volume estimated from the high speed film data at the time when Phase I has just been completed. The two agree to within 10%.

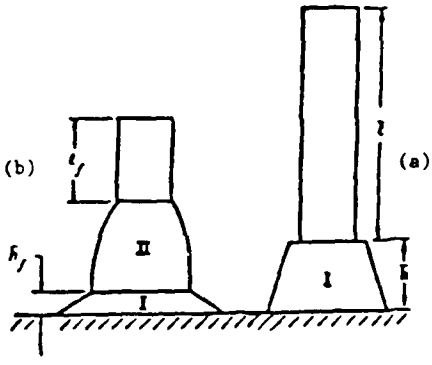


Figure 11: An exaggerated view of the mushroom geometry (a) at the end of Phase I deformation, and (b) the end of the event. The mushroom suffers considerable axial compression during Phase II deformation.

Using the observation in the previous paragraph, we can say that volume contained in the undeformed section at $t = \bar{t}$ is $\bar{\ell} A_0$. Since the volume contained in the mushroom is V, it follows that

$$\bar{\ell} = L \left(1 - \frac{V}{LA_0}\right) \tag{32}$$

where $LA_0$ is the volume of the undeformed specimen. This estimate for the undeformed section length at the end of Phase I is quite sound.

## RESULTS

The two-phase theory presented in the previous sections provides for a useful interpretation of the Taylor impact test. In this section, we show how the post-test measurements can be used in the theory to predict dynamic yield stresses and plastic wave speeds. We will deal with each phase separately, beginning with Phase II.

Certain key variables may be assumed to be continuous at the interface between the phases and the values of these variables are assumed to be known. $\ell$, h, s, and v are all assumed to be continuous at $t = \bar{t}$. From the post-test measurements, we can produce a very reliable estimate for $\bar{\ell}$ by equation (32). We know that $\bar{s} = v_0 \bar{t}$ and $\bar{h} = L - \bar{\ell} - \bar{s}$. Hence, when $\bar{t}$ is known, all of the appropriate lengths and displacements are known. We have reason to believe that $\bar{t}$ is roughly constant for impacts involving the same material against the same anvil. Specifically, $\bar{t}$ is a function of the specimen diameter and the specimen material, provided that the impact velocities are sufficiently high. A heuristic argument can be presented which justifies this conclusion. When the impact pressures are high enough to cause the radial relief waves to propagate at the same speed, the time for communication with the free boundary is constant. The interface time, $\bar{t}$, is a function of the time for the radial stress waves to return from the free surface, reflect from the specimen/anvil interface, and to interact with the longitudinal plastic wave front. High pressure equation of state data such as that presented by Walsh, Rice, McQueen, and Yarger [11] and Marsh [12] support this conclusion. The adiabatic compressibility

$$k_s = \frac{-1}{V} \left(\frac{\partial V}{\partial \rho}\right)_s \tag{33}$$

is nearly constant for a number of important materials. Thus, the rate of propagation of a radial stress wave $\sqrt{1/\rho k_s}$ is nearly constant for pressures that are sufficiently high (say, 2-5 GPa). When the specimen and anvil materials are dissimilar, radially reflected stress waves will reflect from the specimen/anvil interface, combine, and propagate longitudinally to produce an interaction with the plastic wave front that separates the two phases. For thirty caliber rods, the time for this interaction will be roughly constant for a given material.

Accepting the argument just put forward for the interface time $\bar{t}$, we can now estimate all of the lengths at the end of Phase I. Then, we can use the elementary two-phase theory to estimate the stresses and plastic wave speeds for the material during both phases of the deformation.

Before turning to the calculations, we describe the results of three experiments on OFHC copper. The data from these experiments will be processed using the foregoing theory. A complete description of the experimental apparatus and data acquisition techniques is contained in Wilson, House, and Nixon [10]. Figure 12 shows the results of the three tests and is published here with the permission of the authors. All of the specimens were shot from a 30 caliber gun and had an undeformed diameter of 7.60 mm. In two cases (UK145 and JG30), the specimen aspect ratio was 7.5:1. In the other case (JG32), the specimen aspect ratio was 5:1. The data in Figure 12 has been reduced from high speed camera pictures taken during the experiments. The Cordin Camera was operated at a rate of $10^6$ frames per second during JG30 and JG32. The camera was operated at a rate of $3 \times 10^5$ frames per second during UK145. Notice that the trend in the data precisely reflects the two-phase flow hypothesis. Notice, also, that the time for transition between the phases is approximately the same for all three specimens. In the analysis that follows, this time is taken to be $\bar{t} = 9 \times 10^{-6}$ sec.

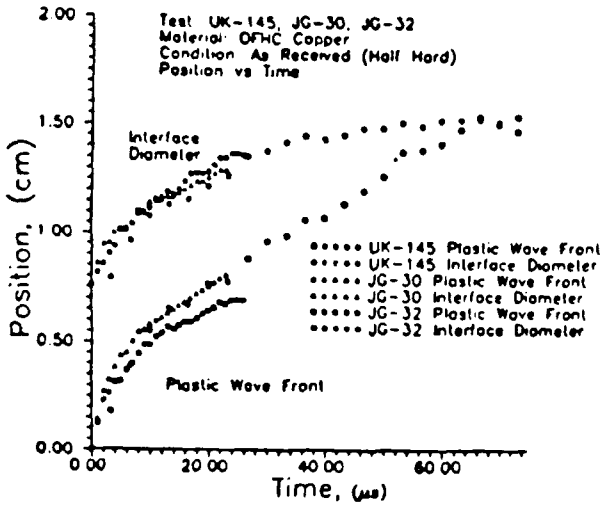


Figure 12. Plastic wave motion and radial growth curves for three impact experiments on OFHC copper. The impact speeds are roughly the same. Secondary plastic flow proceeds with constant wave speed, $\lambda$. The details of these experiments are contained in [10].

First, we will present the results of the calculations for Phase II for the three OFHC copper tests. The Phase II theory is developed by extending equations (26) and (28) to the interface between the phases. When this is done, they become

$$\ell = \ell_f \left[ \frac{Y_{2/\rho}}{Y_2/\rho - \lambda(1-k)v_0 - k(1-k)v_0^2} \right]^{\frac{1}{2(1-k)}}$$

$$\times \left[ \frac{q-\lambda(1k)}{q+\lambda(1-k)} \; \frac{q+\lambda(1-k) + 2k(1-k)\, v_0}{q-\lambda(1-k) - 2k(1-k)\, v_0} \right]^{\frac{1}{q}} \qquad (34)$$

and

$$t_f - \bar{t} = \frac{h_f - \bar{h}}{\lambda} = \int_0^{v_0} \frac{\ell \, dv}{(\lambda+v) f(v)} \qquad (35)$$

where $\ell$ is taken from (26) and $f(v)$ is defined in (25). These two equations and (30) comprise the system for the analysis of Phase II deformation. The unknowns are $Y_2$, $\lambda$, and k. As mentioned earlier, $\bar{t} = 9 \times 10^{-6}$ sec.

The input data from the post-test measurements is given in Table 1.

TABLE 1

| Test # | Impact Velocity m/s | L/D | Final Length (inch) | Final Diameter (inch) | Undeformed Length (inch) | Frame Rate (million) | Material Condition |
|---|---|---|---|---|---|---|---|
| UK-145 | 189 | 7.5 | 1.64 | 0.58 | 0.642 | 0.3 | As Received |
| JG-30 | 176 | 7.5 | 1.689 | 0.54 | 0.990 | 1.0 | As Received |
| JG-32 | 200 | 5.0 | 1.092 | 0.58 | 0.683 | 1.0 | As Received |

The results of the Phase II analysis using (34), (35), and (30) are given in Table 2. Comparing the secondary wave speed, these results are in excellent agreement with the experiment.

TABLE 2

| Test # | $V_0$ m/s | $\lambda$ m/s | $Y_2$ MPa | k | $t_f$ μ sec | $\bar{h}$ mm | $\bar{\ell}$ mm | $\bar{Y}$ mm |
|---|---|---|---|---|---|---|---|---|
| UK145 | 189 | 176 | 350 | 0.247 | 117.3 | 6.096 | 1.702 | 49.276 |
| JG30 | 176 | 161 | 305 | 0.213 | 131.1 | 5.588 | 1.575 | 50.038 |
| JG32 | 200 | 196 | 408 | 0.292 | 71.3 | 5.038 | 1.800 | 31.242 |

A least squares fit to the reduced film data in Figure 12 for UK145 and JG30 gives an experimentally observed value of 173 m/s for $\lambda$. Notice that the calculated values for the secondary wave speed for these two tests differ from this experimental value by less than 7%. The average dynamic yield stresses are calculated to be 350 MPa and 305 MPa, respectively. These estimates are entirely reasonable. The static yield stress for this material is roughly 225 MPa by a 0.2% offset on tension test data.

The difference in the predicted Phase II stresses for UK145 and JG30 can be attributed to the difference in average strain rate during Phase II deformation. The terminal time for JG30 is predicted to be about 14 $\mu$s longer than UK145. Hence, the average strain rate must be lower and the dynamic yield stress is correspondingly lower.

The results for JG32 are also quite acceptable. The dynamic yield stress estimate is 408 MPa, which represents an increase of 81% over static yield. This is a reasonable conclusion for a 5:1 specimen. The terminal time is much shorter (71.3 $\mu$s predicted) and this means that the average strain rate during secondary deformation is much higher. Hence, the higher predicted value for $Y_2$. The secondary plastic wave speed is predicted to be $\lambda$ = 196 m/s. This is also entirely reasonable.

The Phase I analysis consists of determining the exponent n from the equation for the initial particle velocity

$$u(0) = u_0 = v_0 \ (1 - n) \tag{36}$$

When the initial particle velocity is known, n can be found from (36).

Having found n, $h_0$, can be determined from the kinematical relation

$$\bar{h} = h_0 \bar{t}^n = L - \bar{l} - \bar{s} = L - \bar{l} - v_0 \bar{t} \tag{37}$$

Since $\bar{l}$ and $\bar{t}$ are known, it follows that $h_0$ can be found from (37). This means that the wave front motion is completely determined.

Estimates for the initial particle velocity have been given by several investigators (e.g. Walsh, Rice, McQueen, and Yarger [11]). Based on their considerations, we may roughly assume that $u_0 = v_0/2$ for a copper rod impacting a steel anvil. Using (36), this leads to n = 1/2. Using this value of n in (37), we can determine $h_0$.

Having determined h = h(t) during Phase I, we can compute the stress from (11), the particle velocity u from (19), and the engineering strain in the mushroom, e, from (20). The strain-rate during mushroom formation can be found by differentiating e in (20). The results of some of these calculations are given in Figures 13, 14, 15, and 16.

Figure 13 shows the comparison of the predicted wave front position with the experimental observations from reduced film data during the early stage of deformation. The comparison is very favorable.

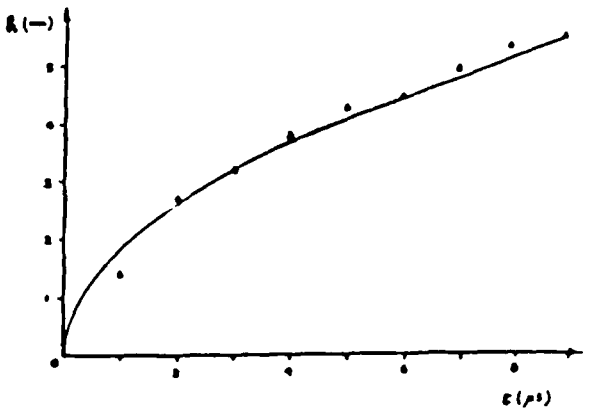


Figure 13. A comparison of the theoretical prediction for plastic wave front position as a function of time (solid curve) with the experimentally observed position Δ. The experimental data is from JG30 and the theoretical prediction is for n = 0.5.

In Figure 14, the stress-time curve is given. This calculation has been made by means of equation (10) with n = 0.5. The result here is quite reasonable. Note that $\sigma$ must be initially unbounded because n < 1. But, $\sigma$ quickly reaches a value of about 400 MPa at 8 $\mu$s. These conclusions are for JG30.

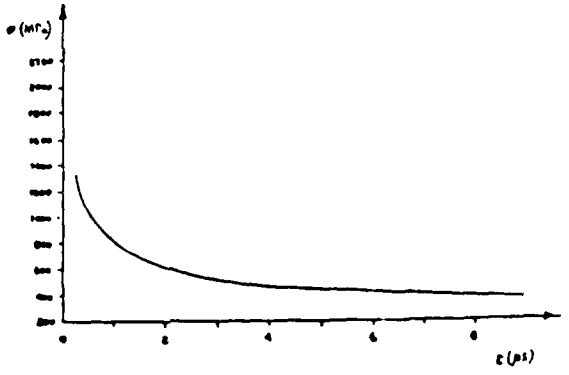


Figure 14. The stress-time curve during Phase I deformation. This result is from equation (11) with n = 0.5. The post-test data is from JG30. Although this stress is compressive, it has been displayed on a positive ordinate for convenience.

As indicated earlier, the strain-rate during Phase I deformation can also be calculated from (20). This result is presented in Figure 15. For convenience, $\dot{e}$ has been plotted as a positive ordinate, although it is negative.

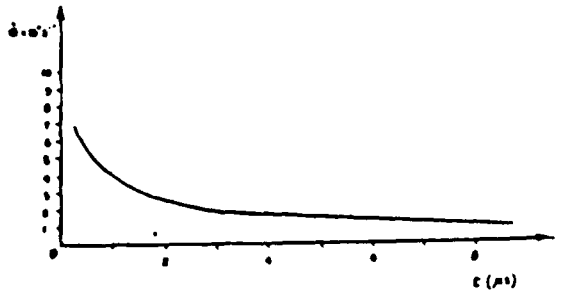

Figure 15. The strain-rate vs. time curve during Phase I deformation. The strain-rate shown here is the result of differentiating equation (20) and using the data from JG30 with n = 0.5.

The results from Figures 14 and 15 can be combined to given an interesting result. Since the stress and strain-rate during Phase I deformation are known as explicit functions of time, time can be algebraically eliminated to produce a stress/strain-rate diagram. Note the form of this graph in Figure 16.

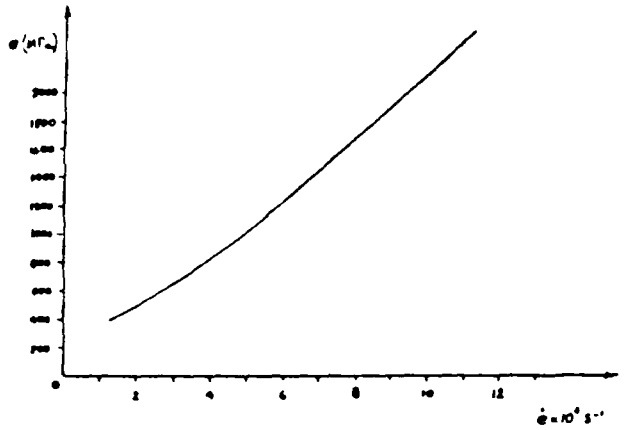

Figure 16. Stress/strain-rate diagram as predicted by the Phase I theory for JG30 and n = 0.5. The relationship is nearly linear.

The stress/strain-rate diagram shown above is carried out beyond the point where it is meaningful for copper. However, it is interesting to note that the curve in nearly linear, even while the strain is varying throughout Phase I. This interesting conclusion has been reported in several places for constant strain (e.g., see Follenbee and Kocks [13]).

We close this section with one final comparison with the experiment. In Figure 17 a comparison between the diameter growth curve for the mushroom and the theoretical prediction is given.

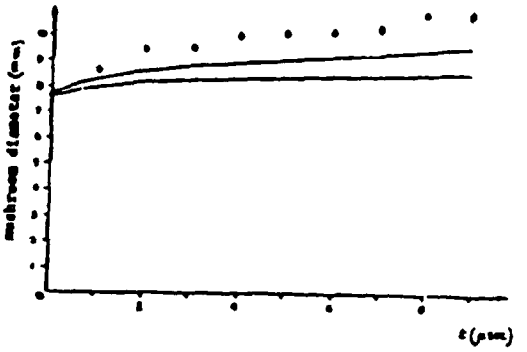

Figure 17. Comparison between experimentally observed mushroom diameter and Phase I model prediction (lower solid curve). The improved estimate using the frustrum of a cone approximation is the upper solid curve.

The growth of the mushroom predicted by the theory is low when compared to the reduced film data from JG30. However, as pointed out in the section on Phase I deformation, and described in Figure 7, this is to be expected. An improvement can be achieved by replacing the cylindrical mushroom section by the frustrum of a cone with the same volume. This, evidently, reduces the disparity between theory and experiment. But, as pointed out earlier, even with this improvement, the results cannot be expected to agree precisely with the experiment.

## CONCLUSION

The theory presented in the preceding sections and the supporting experimental evidence have provided some new insight and improved predictive capability for the Taylor test. The important thing to remember is that all of this was accomplished without sacrificing much of the mathematical simplicity of the original Taylor theory [1] or the recent theories proposed by us [3,6,7].

The new two-phase theory can be used to explain the deficiencies of the elementary theories. For example, consider the perfect plasticity theory proposed by us [3]. For the three OFHC copper tests discussed in the previous section, the elementary, perfect plasticity theory presented in [3] gives the results in Table 3.

TABLE 3

| Test # | $V_0$ m/s | $\lambda$ m/s | Y MPa | $t_f$ $\mu$ sec |
|---|---|---|---|---|
| UK143 | 189 | 201 | 476 | 125.1 |
| JG30 | 176 | 200 | 456 | 126.6 |
| JG32 | 200 | 219 | 539 | 78.8 |

These estimates are somewhat high for both the dynamic yield stress Y and the plastic wave speed $\lambda$. We can now see why the wave speed is high for the elementary model. For example, the terminal time for JG30 is $t_f$ = 131.1 $\mu$s from the two phase model and $t_f$ = 126.6 $\mu$s from the elementary model. Yet, through post-test measurements both h-t curves are required to pass through $h_f$ when $t = t_f$. The result of forcing the elementary mathematical model to conform to this measurement is to overestimate the plastic wave speed for the material in question. This situation is described in Figure 18. Notice that by forcing the plastic wave speed to be constant throughout the entire event, we must overestimate it.

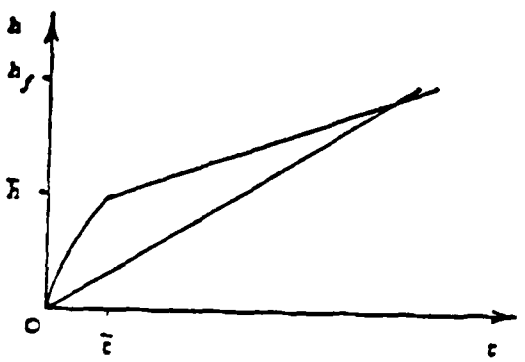


Figure 18. A comparison between the plastic wave front motion for the two phase model (upper curve) and the elementary single phase model (straight line) [3]. The slope of the single straight line through the origin exceeds the slope of the secondary straight line.

The increase in plastic wave speed produces a corresponding increase in the estimate of dynamic yield stress. This, coupled with the fact that radial inertia effects have been neglected, produces inflated values for the dynamic yield stresses.

Future work will deal with corrections for radial inertia during Phase I deformation. Such corrections are only necessary and meaningful during mushroom formation where the strain-rates are very high. During Phase II deformation, the average strain-rates are substantially lower and compensation for radial inertia is not required.

REFERENCES


1. G. I. Taylor, "The Use of Flat-Ended Projectiles for Determining Dynamic Yield Stress," Proc. Roy. Soc. London, Ser. A., 194, 289, 1948.

2. J. F. Bell, "Study of Initial Conditions in Constant Velocity Impact," J. Appl. Phys., 31, 2188 (1960).

3. S. E. Jones, P. P. Gillis, and J. C. Foster, Jr., "On the Equation of Motion of the Undeformed Section of a Taylor Impact Specimen," J. Appl. Phys., 61, 499, 1987.

4. J. J. Molitoris, "The Dynamics of Projectile Impact," Final Report, USAF-UES Summer Faculty Research Program, 1988.

5. J. W. House, "Taylor Impact Testing," AFATL, TR-89-41.

6. P. P. Gillis, S. E. Jones, and M. Dehn, "Some Further Results on the Taylor Impact Test," Mechanics of Materials, 6, 293, 1987.

7. S. E. Jones, P. P. Gillis, J. C. Foster, Jr., and L. L. Wilson, "Interpretations of the Taylor Impact Test," ASME Energy Technology Conference, Houston, 1989.

8. D. Eaton, J. B. Hawkyard, and W. Johnson, "The Mean Dynamic Yield Strength of Copper and Low Carbon Steel at Elevated Temperature from Measurements of the "Mushrooming" of Flat-Ended Projectiles," Int. J. Mech. Sci., 10, 929, 1968.

9. W. Johnson, Impact Strength of Materials, Edward Arnold (Publishers) Ltd., London, 1972, p. 236.

10. L. L. Wilson, J. W. House and M. Nixon, "Analysis of Time Resolvable Data from Cylinder Impact Tests," AFATL TR-89-76.

11. J. M. Walsh, M. H. Rice, R. G. McQueen, and F. L Yarger, "Shock-Wave Compression of Twenty-Seven Materials," Physical Review, 108, 1957.

12. S. P. Marsh, LASL Shock Hugoniot Data, University of California Press, 1980.

13. P. S. Follansbee and U. F. Kocks, "A Constitutive Description of the Deformation of Copper Based on the Use of the Mechanical Threshold Stress as an Internal State Variable," Acta Metall., 36, 81, 1988.